Talanta 235 (2021) 122694

Contents lists available at ScienceDirect

Talanta

journal homepage: www.elsevier.com/locate/talanta

Ninhydrin as a novel DNA hybridization indicator applied to a highly reusable electrochemical genosensor for *Candida auris*

Pedro H.G. Guedes [a], Jéssica G. Brussasco [a], Anna C.R. Moço [a], Dayane D. Moraes [a], José M. R. Flauzino [a], Luiz F.G. Luz [b], Margarete T.G. Almeida [c], Márcia M.C.N. Soares [d], Ronaldo J. Oliveira [e], João M. Madurro [b], Ana G. Brito-Madurro [a,*]

[a] Institute of Biotechnology, Federal University of Uberlândia, Uberlândia, Brazil
[b] Institute of Chemistry, Federal University of Uberlândia, Uberlândia, Brazil
[c] Faculty of Medicine of São José do Rio Preto, São José do Rio Preto, Brazil
[d] Adolfo Lutz Institute, Regional Laboratory in São José do Rio Preto, Brazil
[e] Department of Physics, Institute of Exact, Natural Sciences and Education, Federal University of Triângulo Mineiro, Uberaba, Brazil

ARTICLE INFO

Keywords:
Candida auris
Fungal pathogens
Diagnosis
Point of care
Electrochemical genosensor
Ninhydrin

ABSTRACT

This work reports a simple strategy for *Candida auris* genomic DNA (gDNA) detection, a multi-resistant fungus associated with nosocomial outbreaks in healthcare settings, presenting high mortality and morbidity rates. The platform was developed using gold electrode sensitized with specific DNA capture probe and ninhydrin as a novel DNA hybridization indicator. The genosensor was able to detect *C. auris* in urine sample by differential pulse voltammetry and electrochemical impedance spectroscopy. The biosensor's analytical performance was evaluated by differential pulse voltammetry, detecting up to 4.5 pg μL^{-1} of *C. auris* gDNA in urine (1:10, V/V). Moreover, the genosensor was reused eight times with no loss in the current signal response. The genosensor showed selectivity and stability, maintaining 100% of its response up to 80 days of storage. In order to analyze interactions of single and double-stranded DNA with ninhydrin, SEM, AFM and molecular dynamics studies followed by docking simulations were performed. Theoretical calculations showed ninhydrin interactions more favorably with dsDNA in an A-T rich binding pocket rather than with the ssDNA. Therefore, the proposed system is a promising electrochemical detection device towards a more accurate detection of *C. auris* gDNA in biological samples.

1. Introduction

Fungal pathogens are estimated to be a major cause for human morbidity and mortality, infecting billions and killing over 1.6 million people worldwide per year [1,2]. The emergence of drug-resistant pathogens is a medical concern issue since these microorganisms may cause severe human diseases [3].

Candida auris is a multi-resistant fungus, associated with nosocomial outbreaks in healthcare settings. It is a rising threat to public health, presenting high mortality and morbidity rates [4]. *C. auris* outbreaks have already been notified in COVID-19 hospitals [5] and patients with COVID-19 infected with this fungus have been reported [6]. Therefore, every health care facility should be severely monitored in order to contain this imminent threat since SARS-CoV-2 and *C. auris* combination might be deadly [7].

The *C. auris* accurate identification by phenotypic methods may be challenging [8] and this fungus cannot be identified using commonly commercial systems, and thus a suitable treatment is delayed [9]. Moreover, conventional laboratory techniques can lead to misidentification and improper handling, making it difficult to control the spread of *C. auris* in healthcare environments [10].

One of the most recent methods to detect pathogens is the development of biosensors [11]. Among biosensors, electrochemical genosensors stand out as devices with sequence-specific DNA detection, allowing them to precisely identify pathogens [12]. They present superior advantages due to their low cost, rapid results, selectivity, miniaturization capacity, instrumental and operational simplicity compared to most analytical techniques, and therefore offering the possibility for point-of-care (POC) diagnosis [13].

Electrochemical genosensors often utilize indirect or label-based

* Corresponding author.
E-mail address: agbrito@ufu.br (A.G. Brito-Madurro).

https://doi.org/10.1016/j.talanta.2021.122694
Received 24 April 2021; Received in revised form 2 July 2021; Accepted 6 July 2021
Available online 8 July 2021

detection methods, monitoring DNA hybridization by distinct electrochemical responses of a redox indicator which interact specifically with either single stranded (ss) or double stranded (ds) DNA [14,15].

Ninhydrin (1,2,3-Triketohydrindene monohydrate, NHN) is a well-known molecule commonly used for amino acid analysis due to its interaction with amino groups in protein and peptides [16]. In addition, ninhydrin has been reported to interact with heterocyclic nucleobases [17] and modify guide RNA in CRISPR systems [18].

However, ninhydrin potential as an electroactive hybridization indicator as well as the bioinformatics on its interaction with ssDNA and dsDNA applied to a genosensor technology has not been examined yet.

Therefore, the present paper reports a novel and reusable electrochemical genosensor capable of sensitive and selective detection of *C. auris* gDNA by differential pulse voltammetry and electrochemical impedance spectroscopy. The DNA biosensor presented a remarkable regeneration ability and 100% of its signal response was maintained up to 80 days of storage. This straightforward approach is the first electrochemical genosensor for *C. auris* gDNA detection using ninhydrin as a novel hybridization indicator.

2. Material and methods

2.1. Chemicals and biomolecules

All chemicals were used without prior purification and presented analytical grade. High purity water (18.2 MΩ cm, Master System, Gehaka, Brazil) was used to prepare solutions which were deoxygenated by bubbling ultra-pure nitrogen before electrochemical measurements. Potassium chloride (99%, KCl) was purchased from Neon. Sulfuric acid (98%, H_2SO_4), $K_4[Fe(CN)_6]$ and $K_3[Fe(CN)_6]$ were obtained from Sigma-Aldrich Chemical, USA (ACS purity). Dibasic sodium phosphate (99%, Na_2HPO_4) and monobasic sodium phosphate (99%, NaH_2PO_4) were acquired from Synth. Ninhydrin (ACS reagent) was purchased from Sigma Aldrich.

The DNA probe (CAU1S) sequence was carefully designed using the National Center for Biotechnology Information (NCBI) data bank. The sequence can be identified by its RID (4TCMJD2901R). CAU1S (5'-(HS) AACAAAACGAAAAAAAAAGCGTAGA-3′) was purchased from Alpha DNA (Canada) and a stock solution (1 mmol L^{-1}) was prepared using deionized water. *C. auris* gDNA was extracted using the in-house method [19]. The purity and quality of the samples were evaluated by spectrophotometry. To obtain a positive sample, human urine free of *C. auris* was diluted using deionized water (1:10, V/V) and enriched with gDNA of the fungus. For selectivity tests, nucleic acids from different organisms such as Zika virus, *Escherichia coli* and *Neisseria meningitidis* were used.

2.2. Instrumentation

Electrochemical measurements were performed using Differential Pulse Voltammetry (DPV) in a potentiostat CHI 760C (CH Instruments, USA). Autolab potentiostat/galvanostat PGSTAT302 N (Eco Chemie, Utrecht) with FRA module were used to perform Electrochemical Impedance Spectroscopy (EIS), using Nova 2.1.3 software. All electrochemical experiments were conducted using a three-electrode electrochemical cell, 2 mm diameter gold working electrodes, platinum wire as counter electrode and Ag/AgCl/Cl^- (3.0 mol L^{-1} KCl) as reference electrode. The surface morphology of the electrodes was assessed by scanning probe microscopy (Model 5100 N, Hitachi), performed in the dynamic force microscope (DFM) mode, and by scanning electron microscopy (SEM) on an EVO MA10 Zeiss microscope.

2.3. Molecular modeling and computational protocol

The initial ssDNA and dsDNA structures were generated by proto-Nucleic-Acid Builder (pNAB) [20] and submitted to CHARMM-GUI [21] in order to generate the input files for the molecular dynamic simulations. Equilibration, 10-ns production runs and analyses were conducted with GROMACS 5.1.4 [22] with similar protocol as previously published [23,24]. Ligand-binding hot spots were characterized with FTMap [25]. Molecular docking was performed with the GOLD (Genetic Optimization for Ligand Docking) 2020 [26] with the same protocol as previous study [27]. A more complete protocol is presented in the Supplementary Information section.

2.4. Fabrication of genosensor and Candida auris gDNA detection

Gold electrodes (Au) were submitted to mechanical and electrochemical conditioning. For mechanical preconditioning, Au were immersed in an ethanol solution (70%) and ultrasonicated for 10 min. Mechanical polishing was carried out using alumina slurry (0.3 μm), after being immersed in deionized water and sonicated for 2 min. Electrochemical preconditioning was performed using cyclic voltammetry in H_2SO_4 (0.5 mol L^{-1}), 6 cycles with potential ranging from 0.0 V to +1.4 V, 50 mV s^{-1}.

Probe immobilization was carried out by dripping 3.0 μL of CAU1S (20 μmol L^{-1}, pH 7.4) and after 30 min, Au/CAU1S was immersed in phosphate buffer saline (PBS) solution (0.1 mol L^{-1}, pH 7.4), for 7 s so that non-adsorbed capture probes are washed out.

CAU1S concentration used in the electrochemical detection was optimized by direct detection, monitoring the oxidation of guanosine and adenosine. DPV in PBS solution (0.1 mol L^{-1}, pH 7.4) was conducted with potential ranging from 0.6 V to +1.4 V, modulation amplitude 60 mV, interval time 0.2 s, scan rate 30 mV s^{-1}; interval time 0.2 s.

Hybridization procedure was performed by dripping 5 μL of urine (1:10, V/V) enriched with *C. auris* gDNA onto Au/CAU1S surface and conditioned in 55 °C for 20 min. Subsequently, Au/CAU1S:gDNA were immersed in PBS solution (0.1 mol L^{-1}, pH 7.4) for 7 s to wash unbound DNA from the Au/CAU1S surface.

Indirect detection was carried out by adding 5 μL of ninhydrin solution (100 μmol L^{-1}) onto Au/CAU1S:gDNA surface. After 10 min at room temperature, the unbounding ninhydrin was removed using deionized water by immersion of Au/CAU1S:gDNA/NHN for 7 s. DPV was recorded with potential ranging from −0.7 V to +0.2 V, modulation amplitude 60 mV, interval time 0.2 s, scan rate 30 mV s^{-1}; interval time 0.2 s using an electrolyte PBS solution (0.1 mol L^{-1}, pH 7.4). As proof of concept for DPV results, EIS studies using anionic probe $K_4[Fe(CN)_6]$/$K_3[Fe(CN)_6]$ (5 mmol L^{-1}) in KCl solution (0.1 mol L^{-1}) were carried out immediately after DNA hybridization with an open circuit, a frequency ranging from 10 kHz to 0.1 Hz and amplitude of 10 mV.

The calibration curve was constructed by varying *C. auris* gDNA concentration in urine diluted using deionized water (1:10, V/V) ranging from 4.5 pg μL^{-1} to 45 ng μL^{-1}. Differential pulse voltammograms were recorded as the analytical signal by indirect detection using ninhydrin as indicator in PBS solution (0.1 mol L^{-1}, pH 7.4).

2.5. Selectivity, regeneration and stability assays

In order to evaluate the selectivity of the genosensor, human urine sample (1:10, V/V) was enriched with nucleic acids from Zika virus, *Neisseria meningitidis* and *Escherichia coli* at the same concentration of the positive sample, *C. auris* gDNA (0.45 ng μL^{-1}) and added onto Au/CAU1S. For regeneration studies, Au/CAU1S:gDNA of *C. auris* was washed in PBS solution, pH 7.4, by immersion for 30 s. Subsequently, in order to de-hybridize *C. auris* gDNA from Au/CAU1S, the surface was immersed in water at 90 °C for 5 min. This procedure was repeated 8 times. After, DPV analysis were conducted using ninhydrin as an indicator. The stability of the genosensor was evaluated by maintaining Au/CAU1S bioelectrodes at 8 °C for 80 days. Then, electrochemical response was evaluated up to 80 days of storage. For selectivity, regeneration and stability assays, DPV was performed in PBS solution (0.1 mol L^{-1}, pH 7.4) and the oxidation peak of ninhydrin was monitored.

2.6. Statistics and data presentation

Arithmetic mean value ± standard deviation is represented for numeric numbers, performed in triplicate measurements. Histogram graphs were plotted using Prism Graph 6.0 and voltammograms using Origin 7 after baseline subtraction.

3. Results and discussion

3.1. Optimization of probe DNA immobilization on gold electrode

Efficient DNA probe immobilization onto an electrode surface plays an important role in the overall performance of genosensors [28]. Therefore, suitable probe orientation and its optimal concentration are relevant parameters to achieve a high-quality biosensor [29]. Three different concentrations of CAU1S DNA probe were evaluated by direct detection, monitoring guanosine and adenosine oxidation as shown in Fig. 1.

According to literature, DNA can be oxidized onto gold electrodes [30,31]. Fig. 1A shows two oxidation peaks at $E_p = +0.9$ V and +1.3 V corresponding to guanosine and adenosine oxidation peaks, respectively, at 20 μmol L^{-1} of CAU1S. In addition, guanosine presented $i_p = 9.70 \pm 0.3$ μA and adenosine $i_p = 2.1 \pm 0.1$ μA, according to Fig. 1B. No oxidation peak was detected for the other tested concentrations (10 μmol L^{-1} and 5 μmol L^{-1}). Therefore, CAU1S at 20 μmol L^{-1} was used in all assays as the optimal DNA probe concentration.

AFM imaging allows the investigation of biomolecules attached to the solid substrate. CAU1S immobilization was also evaluated by scanning probe microscopy. Bare gold electrode showed a typical rough surface with small valleys presenting quadratic roughness coefficient (Rq) of 8.8 ± 1 nm, according to Fig. 1C. After the addition of CAU1S, a decrease in the Rq value (4.3 ± 0.3 nm) was observed (Fig. 1D). The decrease in the roughness value may be due the thiolated DNA probe which occupies the small valleys of the electrode surface, tending to form a smoother surface [32]. Also, studies on ssDNA physical properties indicate high conformational flexibility in solution [33] or onto solid surfaces, fitting more easily into the grooves of these surfaces [34].

3.2. Performance evaluation of genosensor

3.2.1. Calibration curve and sensibility

Candida auris is often detected in urine samples from contaminated people [35,36]. In this study, human urine sample (1:10, V/V) was enriched with different concentrations of *C. auris* gDNA and a calibration curve was constructed in order to evaluate the sensitivity of the genosensor. Indirect detection was carried out by DPV, monitoring ninhydrin oxidation peak as presented in Fig. 2.

The ninhydrin indicator used to monitor the duplex formation (CAU1S:gDNA) presented an increase in the oxidation peak $E_p = -0,25$ V (vs. Ag/AgCl/Cl^- (KCl 3.0 mol L^{-1}) as the concentration of *C. auris* gDNA increases in urine sample, according to Fig. 2A. It appears to present a higher affinity towards dsDNA. This behavior is also observed in other hybridization indicators, such as ethidium bromide [37] and Ru $(NH_3)_6]Cl_3$ [38] which present high costs and potential toxicity [39]. As an alternative, ninhydrin offers great advantages as an electrochemical DNA hybridization indicator, such as low oxidation potential required (−0.25 V) and it is an economical and environment friendly molecule [40]. The biosensor detected up to 4.5 pg μL^{-1} with linear range from 45 ng μL^{-1} to 4.5 pg μL^{-1} of gDNA in real sample, with equation i_p (nA) = 1756–147.92 (nA/g μL^{-1}) * (–log[gDNA]) (g μL^{-1}) and $R^2 = 0.99953$

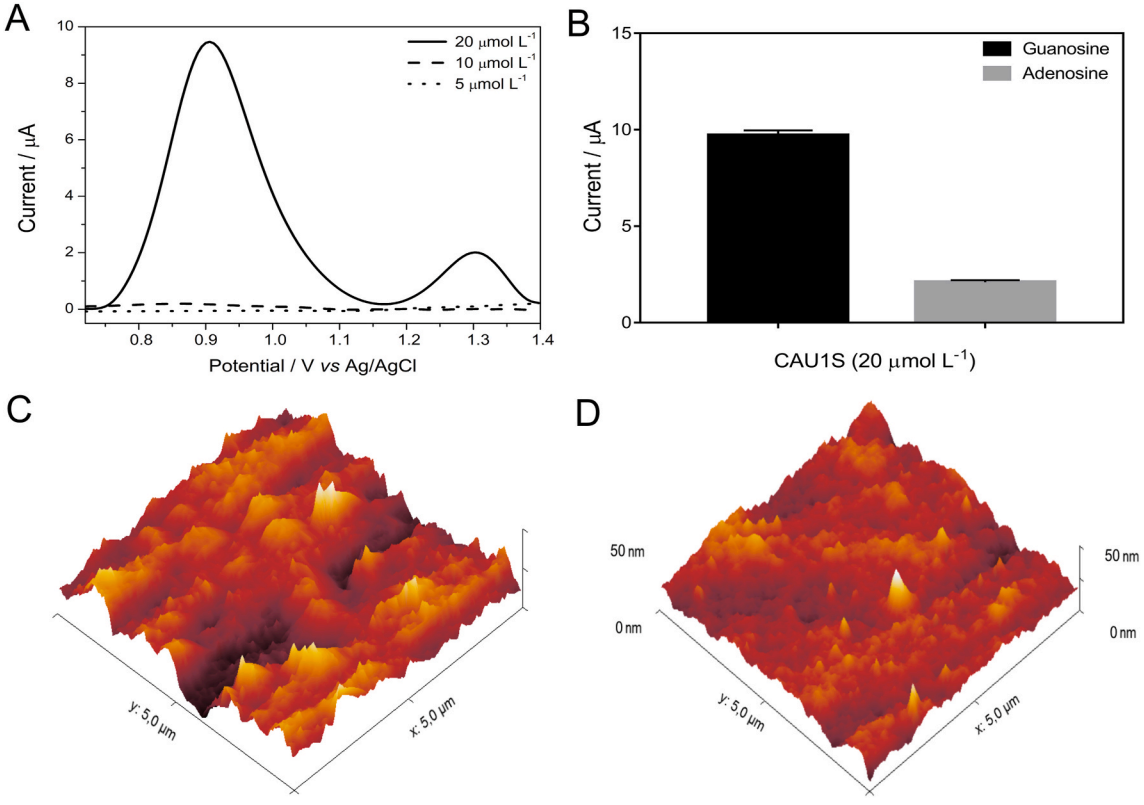

Fig. 1. Optimization of CAU1S DNA probe concentration onto gold electrodes. A) Differential pulse voltammograms for guanosine and adenosine oxidation at concentrations 5 μmol L^{-1} (···), 10 μmol L^{-1} (–) and 20 μmol L^{-1} (–) in PBS solution (0.1 mol L^{-1}, pH 7.4). Potential scan from 0.6 V to +1.4 V; scan rate 30 mV s^{-1}; modulation amplitude 60 mV; interval time 0.2 s. B) Histogram for current values to the guanosine and adenosine oxidations at concentrations 20 μmol L^{-1}. AFM images of the bare gold electrode (C) and Au/CAU1S (D). (For interpretation of the references to colour in this figure legend, the reader is referred to the Web version of this article.)

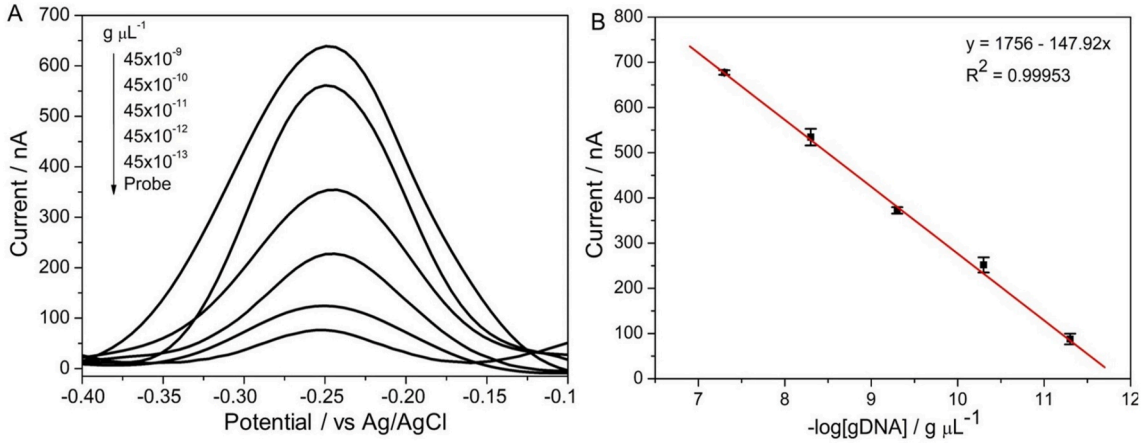

Fig. 2. Electrochemical response for indirect detection of *C. auris* gDNA added in urine (1:10, V/V) at different concentrations monitoring ninhydrin oxidation peak and the calibration curve. A) Differential pulse voltammograms recorded in PBS solution (0.1 mol L^{-1}, pH 7.4), in absence or presence of target analyte, varying its concentration (45×10^{-13} g μL^{-1}, 45×10^{-12} g μL^{-1}, 45×10^{-11} g μL^{-1}, 45×10^{-10} g μL^{-1} and 45×10^{-9} g μL^{-1}). Conditions: potential scan from −0.7 V to +0.2 V; scan rate 30 mV s^{-1}; modulation amplitude 60 mV; interval time 0.2 s. B) Calibration plots for the amperometric response.

(Fig. 2B).

3.2.2. Selectivity, reusability and stability

Parameters such as selectivity, regeneration and stability were evaluated by indirect detection, monitoring the current response of ninhydrin oxidation (Fig. 3).

Au/CAU1S genosensor was sensitized with gDNA from non-target pathogens which are also found in urine such as *Candida albicans* [41], Zika virus gRNA [42], *Neisseria meningitidis* [43] and *Escherichia coli* gDNAs [44] at the same concentration of *C. auris* gDNA (0.45 ng μL^{-1}). The genosensor was able to distinguish all non-specific pathogens DNA and presented a similar current value when compared to the probe current response, according to Fig. 3A. *C. albicans* gDNA with $i_p = 70 \pm 2.6$ nA, Zika virus gRNA with $i_p = 57.7 \pm 1.5$ nA, *N. meningitidis* gDNA

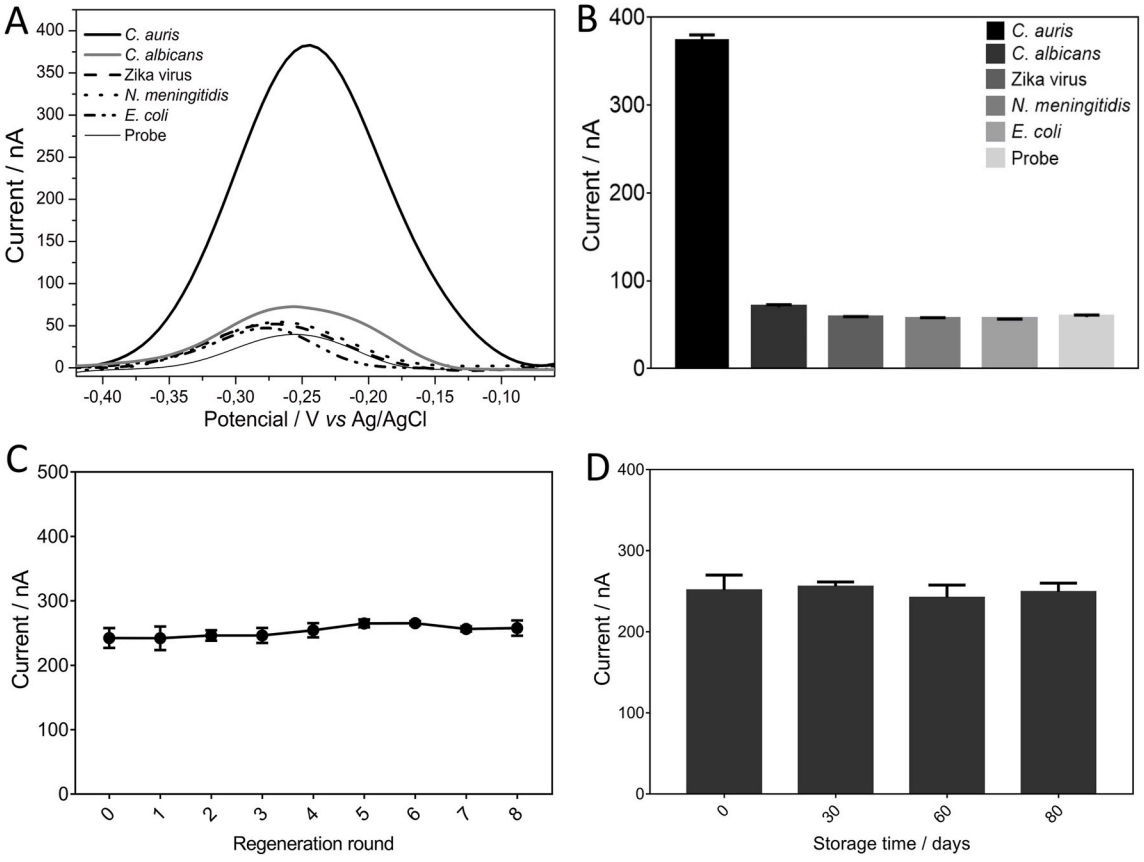

Fig. 3. A) Differential pulse voltammograms and B) histogram of current value for the detection of *C. auris* gDNA and non-specific biomolecules: *C. albicans*, Zika virus gRNA, *N. meningitidis* and *E. coli*. C) Relation between i_p and regeneration rounds. D) Relation between i_p and storage time of the genosensor. DPV was recorded in PBS solution (0.1 mol L^{-1}, pH 7.4); potential scan from −0.7 V to +0.2 V; scan rate 30 mV s^{-1}; modulation amplitude 60 mV; interval time 0.2 s. Ninhydrin oxidation peak was monitored in all experiments.

with i_p = 56.3 ± 1.5 nA and *E. coli* gDNA with i_p = 55.7 ± 0.6 nA, presented 5.3-fold, 6.5-fold, 6.6-fold and 6.7-fold decrease in peak current variation, respectively, comparing to the positive control (i_p = 373 ± 9.9 nA), as observed in Fig. 3B. In addition, a misidentification of *C. auris* as *N. meningitidis* and *C. albicans* has been reported [45,46]. Nevertheless, the present genosensor showed superior selectivity since it was able to accurately discriminate *C. auris* from *N. meningitidis* and *C. albicans*.

In order to obtain a cost-effective point-of-care diagnosis, regeneration assay is an important feature to accelerate biosensor commercialization [47], since it evaluates the ability of DNA hybridization reaction to re-occur between gDNA and CAU1S. As result of an effective chemisorption between 5′ thiol labeled DNA probe and the gold surface [48], the genosensor presented high reusability, maintaining 100% of its current response signal over 8 regeneration cycles, according to Fig. 3C. The genosensor's stability was examined by keeping the bioelectrodes at 4 °C over 80 days. Fig. 3D shows the DNA biosensor being able to maintain 100% of its signal response up to 80 days of storage.

C auris is mostly detected by quantitative real-time PCR (qPCR) [49,50]. However, qPCR is a laborious operational procedure which presents some challenges towards a point-of-care diagnosis, including high cost and unstable results [51]. To the best of our knowledge, no electrochemical genosensor for the detection of *C. auris* gDNA in urine samples using ninhydrin as DNA hybridization indicator has been reported. Therefore, Table 1 presents recently reported methodologies able to identify *C. auris*.

In this work, the developed genosensor showed superior features such as linear range, rapid response and small amount of sample required. In addition, all previously reported detection methods (see Table 1) lack important studies such as stability and regeneration.

3.3. Evaluation of the genosensor by bioinformatics, EIE and morphological analysis

3.3.1. Computational analysis of ninhydrin in complex with DNA

Ninhydrin interactions with DNA were evaluated by theoretical approaches in order to obtain some insights for the DNA-ninhydrin binding mechanism (Fig. 4).

Initially, molecular dynamics simulations were performed with the modeled ssDNA and dsDNA biomolecules with the results presented in Fig. 4A and B, respectively. Fig. 4A and B shows the radius of gyration (R_g) and the total energy of the molecules simulated during a total time of 10 ns? Both structures were reasonably stable during the simulations which reflected the constant R_g and energy along the 10 ns-runs. However, ssDNA was more extended than dsDNA which could be seen by the higher R_g for ssDNA ($R_g \approx 3.0$ nm in A) than for dsDNA ($R_g \approx 2.5$ nm in B), despite of both molecules having the same initial length. R_g is a measure that considers the average atomic position of a molecule in a specific time, thus, ssDNA samples more extended conformations than dsDNA.

Table 1
Comparison of proposed genosensor for *C.auris* gDNA detection with other methodologies.

Methodology	Sample volume	Time of detection	Stability	Regeneration	Reference
Fluorescence	100 µL	60 min	n.a	n.a	[56]
Spectroscopy BCID-FP (GenMark Dx ePlex)	50 µl	100 min	n.a	n.a	[57]
Multiplex PCR and qPCR	4 µl	~79 min	n.a	n.a	[58]
CHROMagar	1 µl	36 h	n.a	n.a	[59]
LAMP	2 µl	90 min	n.a	n.a	[60]
DPV indirect detection	5 µl	32 min	100 days	8 times	This study

Molecular dynamic simulations create conformations by stochastic or diffusive motions on a roughed energy landscape profile [57]. Simulations of Fig. 4A and B resulted in equilibrated and constant-temperature runs. The final conformations are located in local energy minima in which they might be good representatives of the conformation ensemble for the docking analysis with ninhydrin.

The next step would be to perform molecular docking simulations of ninhydrin against the final DNA structures. Although, before that, the initial and final conformations of ssDNA (structures in Fig. 4A) and dsDNA (structures in Fig. 4B) were submitted to the FTMap [25] web server in order to characterize possible binding cavities. In Figure S1 (see Supplementary Information), FTMap predicted the initial conformations of ssDNA (Fig. S1A, left panel) and dsDNA (Fig. S1C, left panel) having a broad distribution of binding sites that were represented by the small molecule decoys bound to the DNAs surfaces. Also, the nonbonded contact rate of the decoys along the nucleic acid sequence of both molecules were broadly distributed with two slightly higher peaks around nucleotides DG9 and DG21, numbering from its 5′- to 3′-end (left panels of Figs. S1B and S1D). However, the equilibrated conformations represented by the final structures resulted in different conformations for both biopolymers. The end-point of the ssDNA simulation resulted in a more extended conformation than its initial structure and the decoys were found more pronounced around nucleotides DA13 and DA18 (right panels of Fig. S1A and S1B). The final dsDNA structure resulted in a slightly smaller conformation than its initial perfect double helix, producing one pronounced binding site around nucleotide DG19. Thereafter, this nucleotide position was chosen to be the major binding cavity as it appears in both nucleic acid structures.

The last snapshot of the molecular dynamic runs of both structures in Fig. 4A and B were submitted to docking simulations with the hybridization indicator ninhydrin. Although the binding site for the docking runs were centered at nucleotide DG19, the binding cavity was sufficiently big (10 Å) to cover some more nucleotides. Generated by the docking simulations, the top-ranked configurations of ninhydrin in complex with ssDNA and dsDNA were chosen for analysis and they are presented in Fig. 4C and D, respectively. Ninhydrin was captured by the two nucleotides (DG19 and DC20) on the ssDNA surface and by an A-T rich region around DA17 of dsDNA that is a more confined binding pocket (surface representation on the right panels in Fig. 4C and D). Hydrogen bonds were the main stabilizing interaction of the hybridization indicator in both DNAs, with an extra hydrogen bond occurring in dsDNA. Also, the dsDNA-ninhydrin complex exhibited an exclusive hydrophobic interaction, represented by the surface of DA15 nucleotide in Fig. 4D. Similar mode of interaction of a compound bound in a A-T rich region of a double strand DNA was also reported in a recent publication [58].

The theoretical calculations suggest that the hybridization indicator ninhydrin has a more favourable interaction with the double helix dsDNA than with the single strand ssDNA. This is in accordance with the experimental results which showed an increased sensitivity of the dsDNA genosensor when compared with ssDNA, revealing ninhydrin as a novel DNA hybridization indicator.

3.3.2. Electrochemical impedance spectroscopy and morphological analysis

The characterization of the Au/CAU1S and Au/CAU1S:*C. auris* gDNA was performed by EIS, SEM and AFM images (Fig. 5).

Au/CAU1S was sensitized with urine samples (1:10, V/V) with or without the enrichment of *C. auris* gDNA (4.5 ng μL^{-1}). In the presence of gDNA, a 4.8-Fold increase in the resistance to charge transfer (R_{CT}) value (25.7 ± 1.4 kΩ) was observed compared to Au/CAU1S/Urine which presented $R_{CT} = 5.3 \pm 0.5$ kΩ, according to Fig. 5B. These findings corroborate with DPV results, after the duplex formation (Au/CAU1S:gDNA), an increase in the amount of DNA on the Au surface is observed, leading to an increase in the R_{CT} value for the positive sample [59].

It was possible to observe different morphologies in the SEM images, with the addition of the positive target (Fig. 5D) causing a change in the

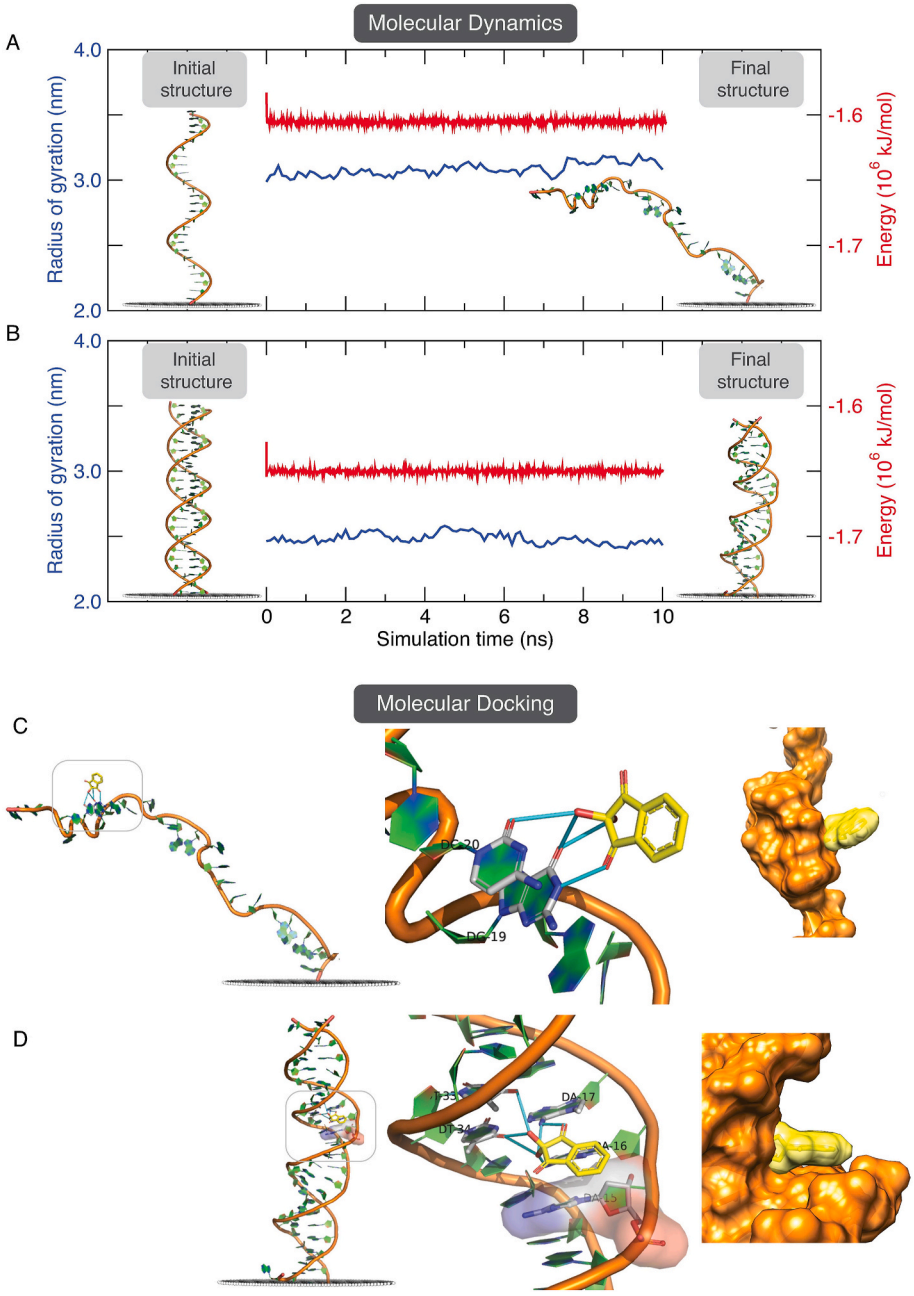

Fig. 4. Theoretical molecular modeling of the interaction between ninhydrin and DNA. Radius of gyration (Rg, blue) and total energy (red) of the molecular dynamics simulations performed with A) ssDNA and B) dsDNA. Initial structures and the final stable configurations of the simulated biomolecules are also presented in A) and B). Molecular docking of ninhydrin (yellow stick) bound with the simulated final structures of C) ssDNA and D) dsDNA. C) and D) also show a close-up of the docked poses on the middle panels and a surface representation on the right panels. Ninhydrin is mainly stabilized via hydrogen bonds (cyan sticks) in both biomolecules, however, only on dsDNA, ninhydrin appears to be stabilized by hydrophobic interactions (surface representation in D). (For interpretation of the references to colour in this figure legend, the reader is referred to the Web version of this article.)

surface of the working electrode, making it more heterogeneous with structures in filamentous form or network-like structures when compared with the negative sample (healthy urine) (Fig. 5C). This may be due to the formation of the DNA duplex after adding the positive target, since double stranded nucleic acids tend to be less flexible than single stranded nucleic acids [60], that can be observed with the formation of different structures on the electrode surface [61]. In both SEM and AFM images it was possible to observe structures approximately 100 nm in size, a common feature in urine samples as a result of drying on solid surfaces [62] and adsorption of solid components present in the sample.

Scanning probe microscopy is also a valuable technique to evaluate DNA hybridization in solid surfaces [63]. The addition of the negative sample resulted in images with lower coefficients of roughness (Rq = 2.9 ± 0.2 nm, Fig. 5E), presenting a predominantly smooth surface with sparse elevation points. In contrast, the electrodes in which the positive samples (urine enriched with gDNA of *C. auris*) were applied showed bigger coefficients of roughness (Rq = 17 ± 1.3 nm, Fig. 5F) and a wavy surface, corroborating with the SEM images. The hybridization of the DNA oligonucleotide probe on the electrode surface with the complementary DNA in the sample creates more prominent clusters and structures on the electrode surface [64].

4. Conclusion

In summary, a facile and straightforward approach to detect *C. auris* gDNA in real samples was described based on the electrochemical detection using ninhydrin as a novel DNA hybridization indicator. The analytical features of biosensor were evaluated and presented a linear response from 4.5 pg μL^{-1} to 45 ng μL^{-1} of gDNA in urine (1:10, V/V) capable of detecting up to 4.5 pg μL^{-1}. Moreover, the genosensor was reused eight times with no loss in the current signal response. The genosensor showed selectivity and stability, maintaining 100% of its response up to 80 days of storage, which indicates shelf-life potential, an

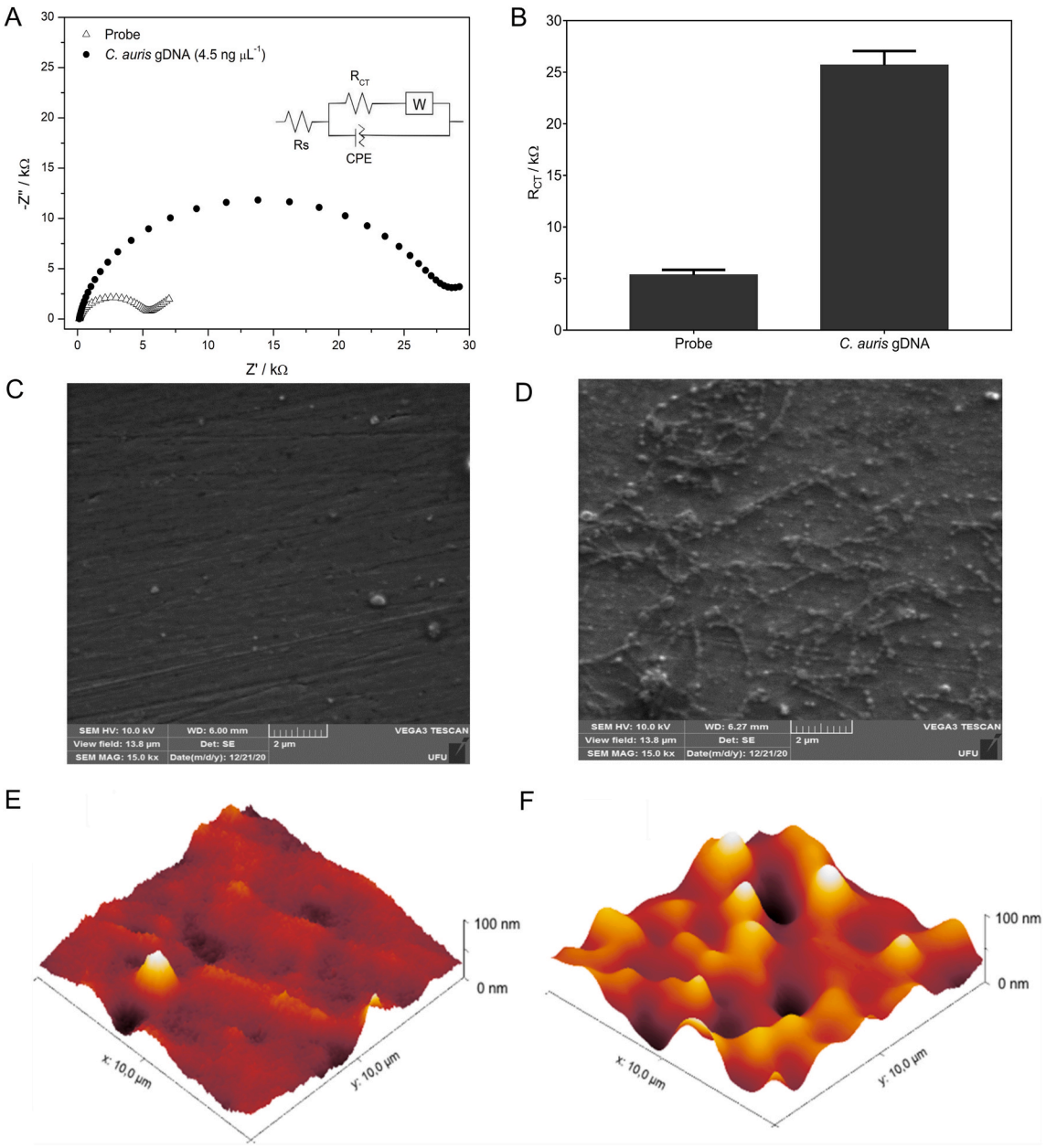

Fig. 5. Electrochemical impedance spectroscopy and morphological analysis. A) Nyquist plots for *C. auris* gDNA detection by EIS. Inset: equivalent circuit, where, R_S, W, R_{CT} and CPE represent the solution resistance, the Warburg diffusion resistance, the charge-transfer resistance and the constant-phase element, respectively. EIS conducted with $K_4[Fe(CN)_6]/K_3[Fe(CN)_6]$ (5 mmol L^{-1}) in KCl solution (0.1 mol L^{-1}), open circuit, frequency ranging from 10 kHz to 0.1 Hz and amplitude of 10 mV. B) Histogram of RCT from the EIS detection of urine (1:10, V/V) without and with *C. auris* gDNA enrichment. SEM and AFM images of Au/CA1US/urine sample without (E) or with (F) *C. auris* gDNA enrichment.

important feature for commercialization. Theoretical calculations support the electrochemical results which reinforce ninhydrin presenting a more favourable interaction with dsDNA than with ssDNA. Therefore, the developed genosensor is a promising electrochemical detection towards the demand for a more accurate identification of *C. auris* gDNA in biological samples.

Credit author statement

Pedro H.G. Guedes: Conceptualization, Methodology, Formal analysis, Investigation, Writing – original draft. Jéssica G. Brussasco: Methodology, Investigation, Writing – original draft. Anna C.R. Moço: Methodology, Investigation, Writing – original draft. Dayane D. de Moraes: Methodology, Investigation, Writing – original draft. José M. R. Flauzino: Methodology, Investigation, Writing – original draft. Luiz F.G. Luz: Methodology, Investigation. Margarete T.G. Almeida: Investigation, C. Auris and C. Albicans sample supply. Márcia N. Soares: Investigation, C. Auris and C. Albicans DNA extraction. Ronaldo J. Oliveira: Molecular Modeling, Conceptualization, Methodology, Investigation, Writing – original draft. João M. Madurro: Conceptualization, Methodology, Formal analysis, Writing – review & editing, Ana G. Brito-Madurro: Supervision, Conceptualization, Methodology, Formal analysis, Writing – review & editing, Funding acquisition.

Declaration of competing interest

The authors declare that they have no known competing financial interests or personal relationships that could have appeared to influence

the work reported in this paper.

Acknowledgements

Financial support was provided by Fundação de Amparo à Pesquisa do Estado de Minas Gerais (FAPEMIG, APQ-00941-14) and Conselho Nacional de Desenvolvimento Científico e Tecnológico (CNPq, 438316/2018-5 and 312328/2019-2). Computational resources were provided by by Núcleo de Computação Científica da Universidade do Estado de São Paulo (NCC/GridUnesp) and Centro Nacional de Processamento de Alto Desempenho em São Paulo (CENAPAD-SP).

Appendix A. Supplementary data

Supplementary data to this article can be found online at https://doi.org/10.1016/j.talanta.2021.122694.

References

[1] R. Hasbun, C.K. Bloch, A. Bhimraj, Neurological Complications of Infections Diseases, Springer, 2021, https://doi.org/10.1007/978-3-030-56084-3_10.
[2] A. König, R. Müller, S. Mogavero, B. Hube, Fungal factors involved in host immune evasion, modulation and exploitation during infection, Cell Microbiol. 23 (2021), https://doi.org/10.1111/cmi.13272.
[3] A. Narmani, R.B. Teponno, M. Arzanlou, F. Surup, S.E. Helaly, K. Wittstein, D. F. Praditya, A. Babai-Ahari, E. Steinmann, M. Stadler, Cytotoxic, antimicrobial and antiviral secondary metabolites produced by the plant pathogenic fungus Cytospora sp. CCTU A309, Fitoterapia 134 (2019) 314–322, https://doi.org/10.1016/j.fitote.2019.02.015.
[4] H. Du, J. Bing, T. Hu, C.L. Ennis, C.J. Nobile, G. Huang, Candida auris: epidemiology, biology, antifungal resistance, and virulence, PLoS Pathog. 16 (2020), e1008921, https://doi.org/10.1371/journal.ppat.1008921.
[5] Centers for Disease Control and Prevention (CDC), Fungal Diseases and COVID-19, 2021 (accessed March 19, 2021), https://www.cdc.gov/fungal/covid-fungal.html.
[6] H. Villanueva-Lozano, R. de J. Treviño-Rangel, G.M. González, M.T. Ramírez-Elizondo, R. Lara-Medrano, M.C. Aleman-Bocanegra, C.E. Guajardo-Lara, N. Gaona-Chávez, F. Castilleja-Leal, G. Torre-Amione, M.F. Martínez-Reséndez, Outbreak of Candida auris infection in a COVID-19 hospital in Mexico, Clin. Microbiol. Infect. (2021), https://doi.org/10.1016/j.cmi.2020.12.030.
[7] R.A. Schwartz, R. Kapila, Cutaneous manifestations of a 21st century worldwide fungal epidemic possibly complicating the COVID-19 pandemic to jointly menace mankind, Dermatol. Ther. 33 (2020), https://doi.org/10.1111/dth.13481.
[8] P.A. Armstrong, S.M. Rivera, P. Escandon, D.H. Caceres, N. Chow, M.J. Stuckey, J. Díaz, A. Gomez, N. Vélez, A. Espinosa-Bode, S. Salcedo, A. Marin, I. Berrio, C. Varón, A. Guzman, J.E. Pérez-Franco, J.D. Escobar, N. Villalobos, J.M. Correa, A. P. Litvintseva, S.R. Lockhart, R. Fagan, T.M. Chiller, B. Jackson, O. Pacheco, Hospital-associated multicenter outbreak of emerging fungus candida auris, Colombia, 2019, Emerg. Infect. Dis. 25 (2016) 1339–1346, https://doi.org/10.3201/eid2507.180491.
[9] A. Ruiz-Gaitán, A.M. Moret, M. Tasias-Pitarch, A.I. Aleixandre-López, H. Martínez-Morel, E. Calabuig, M. Salavert-Lletí, P. Ramírez, J.L. López-Hontangas, F. Hagen, J.F. Meis, J. Mollar-Maseres, J. Pemán, An outbreak due to Candida auris with prolonged colonisation and candidaemia in a tertiary care European hospital, Mycoses 61 (2018) 498–505, https://doi.org/10.1111/myc.12781.
[10] Centers for Disease Control and Prevention (CDC), Candida Auris, 2021 (accessed March 19, 2021), https://www.cdc.gov/fungal/candida-auris/index.html.
[11] A. Mobed, B. Baradaran, M. de la Guardia, M. Agazadeh, M. Hasanzadeh, M. A. Rezaee, J. Mosafer, A. Mokhtarzadeh, M.R. Hamblin, Advances in detection of fastidious bacteria: from microscopic observation to molecular biosensors, TrAC Trends Anal. Chem. (Reference Ed.) 113 (2019) 157–171, https://doi.org/10.1016/j.trac.2019.02.012.
[12] K. Nejati, M. Dadashpour, T. Gharibi, H. Mellatyar, A. Akbarzadeh, Biomedical applications of functionalized gold nanoparticles: a review, J. Cluster Sci. (2021), https://doi.org/10.1007/s10876-020-01955-9.
[13] I.R. Suhito, K.M. Koo, T.H. Kim, Recent advances in electrochemical sensors for the detection of biomolecules and whole cells, Biomedicines 9 (2021) 1–20, https://doi.org/10.3390/biomedicines9010015.
[14] E.E. Ferapontova, Hybridization biosensors relying on electrical properties of nucleic acids, Electroanalysis 29 (2017) 6–13, https://doi.org/10.1002/elan.201600593.
[15] A. Erdem, E. Eksin, G. Kadikoylu, E. Yildiz, Voltammetric detection of miRNA hybridization based on electroactive indicator-cobalt phenanthroline, Int. J. Biol. Macromol. 158 (2020) 819–825, https://doi.org/10.1016/j.ijbiomac.2020.04.168.
[16] A.E. Fazary, K.F. Fawy, M.Z. Bani-Fwaz, T. Sahlabji, H.S.M. Abd-Rabboh, Thermodynamic studies on metal ions – ninhydrin – Glycine interactions in aqueous solutions, J. Chem. Thermodyn. 118 (2018) 302–315, https://doi.org/10.1016/j.jct.2017.12.005.
[17] R. Shapiro, J. Hachmann, The reaction of guanine derivatives with 1,2-dicarbonyl compounds, Biochemistry 5 (1966) 2799–2807, https://doi.org/10.1021/bi00873a004.
[18] S. Wang, H. Huang, J. Liu, L. Wei, L. Wu, W. Xiong, P. Yin, T. Tian, X. Zhou, The manipulation of RNA-guided nucleic acid cleavage with ninhydrin chemistry, Adv. Sci. 7 (2020) 1903770, https://doi.org/10.1002/advs.201903770.
[19] A. Bolano, S. Stinchi, R. Preziosi, F. Bistoni, M. Allegrucci, F. Baldelli, A. Martini, G. Cardinali, Rapid methods to extract DNA and RNA from Cryptococcus neoformans, FEMS Yeast Res. 1 (2001) 221–224, https://doi.org/10.1016/S1567-1356(01)00030-7.
[20] A. Alenaizan, J.L. Barnett, N.V. Hud, C.D. Sherrill, A.S. Petrov, The proto-Nucleic Acid Builder: a software tool for constructing nucleic acid analogs, Nucleic Acids Res. 49 (2021) 79–89, https://doi.org/10.1093/nar/gkaa1159.
[21] J. Lee, X. Cheng, J.M. Swails, M.S. Yeom, P.K. Eastman, J.A. Lemkul, S. Wei, J. Buckner, J.C. Jeong, Y. Qi, S. Jo, V.S. Pande, D.A. Case, C.L. Brooks, A. D. MacKerell, J.B. Klauda, W. Im, CHARMM-GUI input generator for NAMD, GROMACS, AMBER, OpenMM, and CHARMM/OpenMM simulations using the CHARMM36 additive force field, J. Chem. Theor. Comput. 12 (2016) 405–413, https://doi.org/10.1021/acs.jctc.5b00935.
[22] D. Van Der Spoel, E. Lindahl, B. Hess, G. Groenhof, A.E. Mark, H.J.C. Berendsen, GROMACS: fast, flexible, and free, J. Comput. Chem. 26 (2005) 1701–1718, https://doi.org/10.1002/jcc.20291.
[23] F.C. Freitas, P.H.B. Ferreira, D.C. Favaro, R.J. de Oliveira, Shedding light on the inhibitory mechanisms of SARS-CoV-1/CoV-2 spike proteins by ACE2-designed peptides, acs.jcim.0c01320, J. Chem. Inf. Model. (2021), https://doi.org/10.1021/acs.jcim.0c01320.
[24] L.M. Alves, H.L.S. Barros, J.M.R. Flauzino, P.H.G. Guedes, J.M. Pereira, R. T. Fujiwara, T.W.P. Mineo, J.R. Mineo, R.J. de Oliveira, J.M. Madurro, A.G. Brito-Madurro, A novel peptide-based sensor platform for detection of anti-Toxoplasma gondii immunoglobulins, J. Pharmaceut. Biomed. Anal. 175 (2019) 112778, https://doi.org/10.1016/j.jpba.2019.112778.
[25] D. Kozakov, L.E. Grove, D.R. Hall, T. Bohnuud, S.E. Mottarella, L. Luo, B. Xia, D. Beglov, S. Vajda, The FTMap family of web servers for determining and characterizing ligand-binding hot spots of proteins, Nat. Protoc. 10 (2015) 733–755, https://doi.org/10.1038/nprot.2015.043.
[26] M.L. Verdonk, J.C. Cole, M.J. Hartshorn, C.W. Murray, R.D. Taylor, Improved protein-ligand docking using GOLD, Proteins Struct. Funct. Bioinform. 52 (2003) 609–623, https://doi.org/10.1002/prot.10465.
[27] G. Tomasello, I. Armenia, G. Molla, The Protein Imager: a full-featured online molecular viewer interface with server-side HQ-rendering capabilities, Bioinformatics 36 (2020) 2909–2911, https://doi.org/10.1093/bioinformatics/btaa009.
[28] J. Watterson, P.A.E. Piunno, U.J. Krull, Practical physical aspects of interfacial nucleic acid oligomer hybridisation for biosensor design, Anal. Chim. Acta 469 (2002) 115–127, https://doi.org/10.1016/S0003-2670(02)00125-3.
[29] A. Mobed, M. Hasanzadeh, S. Hassanpour, A. Saadati, M. Agazadeh, A. Mokhtarzadeh, An innovative nucleic acid based biosensor toward detection of Legionella pneumophila using DNA immobilization and hybridization: a novel genosensor, Microchem. J. 148 (2019) 708–716, https://doi.org/10.1016/j.microc.2019.05.027.
[30] J.V. da Silva, A.G.B. Madurro, J.M. Madurro, Modified electrode with reduced graphene oxide/poly(3-hydroxyphenylacetic acid): a new platform for oligonucleotide hybridization, J. Solid State Electrochem. 21 (2017) 2129–2139, https://doi.org/10.1007/s10008-017-3601-8.
[31] H.A.M. Faria, V. Zucolotto, Label-free electrochemical DNA biosensor for zika virus identification, Biosens. Bioelectron. 131 (2019) 149–155, https://doi.org/10.1016/j.bios.2019.02.018.
[32] D.A. Oliveira, J.V. Silva, J.M.R. Flauzino, A.C.H. Castro, A.C.R. Moço, M.M.C. N. Soares, J.M. Madurro, A.G. Brito-Madurro, Application of nanomaterials for the electrical and optical detection of the hepatitis B virus, Anal. Biochem. 549 (2018) 157–163, https://doi.org/10.1016/j.ab.2018.03.023.
[33] M.C. Murphy, I. Rasnik, W. Cheng, T.M. Lohman, T. Ha, Probing single-stranded DNA conformational flexibility using fluorescence spectroscopy, Biophys. J. 86 (2004) 2530–2537, https://doi.org/10.1016/S0006-3495(04)74308-8.
[34] A.M. Oliveira-Brett, A.-M. Chiorcea, Atomic force microscopy of DNA immobilized onto a highly oriented pyrolytic graphite electrode surface, Langmuir 19 (2003) 3830–3839, https://doi.org/10.1021/la027047d.
[35] N. Griffith, L. Danziger, Candida auris urinary tract infections and possible treatment, Antibiotics 9 (2020) 898, https://doi.org/10.3390/antibiotics9120898.
[36] A. Al-Rashdi, A. Al-Maani, A. Al-Wahaibi, A. Alqayoudhi, A. Al-Jardani, S. Al-Abri, Characteristics, risk factors, and survival analysis of Candida auris cases: results of one-year national surveillance data from Oman, J. Fungi 7 (2021) 31, https://doi.org/10.3390/jof7010031.
[37] A.C.H. Castro, E.G. França, L.F. De Paula, M.M.C.N. Soares, L.R. Goulart, J. M. Madurro, A.G. Brito-Madurro, Preparation of genosensor for detection of specific DNA sequence of the hepatitis B virus, Appl. Surf. Sci. 314 (2014) 273–279, https://doi.org/10.1016/j.apsusc.2014.06.084.
[38] M. Du, T. Yang, X. Li, K. Jiao, Fabrication of DNA/graphene/polyaniline nanocomplex for label-free voltammetric detection of DNA hybridization, Talanta 88 (2012) 439–444, https://doi.org/10.1016/j.talanta.2011.10.054.
[39] J.I.A. Rashid, N.A. Yusof, The strategies of DNA immobilization and hybridization detection mechanism in the construction of electrochemical DNA sensor: a review, Sens. Bio-Sens. Res. 16 (2017) 19–31, https://doi.org/10.1016/j.sbsr.2017.09.001.
[40] A. Surleva, M. Zaharia, O. Pintilie, I. Sandu, L. Tudorachi, R.V. Gradinaru, Improved ninhydrin-based reagent for spectrophotometric determination of ppb levels of cyanide, Environ. Forensics 17 (2016) 48–58, https://doi.org/10.1080/15275922.2015.1091404.
[41] S. Lal, O. Parkash, P. Kumar, Z.A. Malik, K. Unar, Z. Ahmed, M. Maitlo, A.A. Unar, S. Sapna, Determination of predisposing factors in developing Candida albicans

associated urinary tract infection and antifungal sensitivity profile, J. Pharm. Res. Int. 33 (2021) 40–49, https://doi.org/10.9734/jpri/2021/v33i631188.
[42] M.C. Bonaldo, I.P. Ribeiro, N.S. Lima, A.A.C. dos Santos, L.S.R. Menezes, S.O.D. da Cruz, I.S. de Mello, N.D. Furtado, E.E. de Moura, L. Damasceno, K.A.B. da Silva, M. G. de Castro, A.L. Gerber, L.G.P. de Almeida, R. Lourenço-de-Oliveira, A.T. R. Vasconcelos, P. Brasil, Isolation of infective zika virus from urine and saliva of patients in Brazil, PLoS Neglected Trop. Dis. 10 (2016), e0004816, https://doi.org/10.1371/journal.pntd.0004816.
[43] E. Toh, J.A. Williams, B. Qadadri, A. Ermel, D.E. Nelson, Development of a SimpleProbe real-Time PCR Assay for rapid detection and identification of the US novel urethrotropic clade of Neisseria meningitidis ST-11 (US_NmUC), PloS One 15 (2020), e0228467, https://doi.org/10.1371/journal.pone.0228467.
[44] M.M. Munch, L.C. Chambers, L.E. Manhart, D. Domogala, A. Lopez, D.N. Fredricks, S. Srinivasan, Optimizing bacterial DNA extraction in urine, PloS One 14 (2019), e0222962, https://doi.org/10.1371/journal.pone.0222962.
[45] S. Mahmoudi, S. Agha Kuchak Afshari, S. Aghaei Gharehbolagh, H. Mirhendi, K. Makimura, Methods for identification of Candida auris, the yeast of global public health concern: a review, J. Mycol. Med. 29 (2019) 174–179, https://doi.org/10.1016/j.mycmed.2019.04.004.
[46] C.M. Parra-Giraldo, S.L. Valderrama, G. Cortes-Fraile, J.R. Garzón, B.E. Ariza, F. Morio, M.Y. Linares-Linares, A. Ceballos-Garzón, A. de la Hoz, C. Hernandez, C. Alvarez-Moreno, P. Le Pape, First report of sporadic cases of Candida auris in Colombia, Int. J. Infect. Dis. 69 (2018) 63–67, https://doi.org/10.1016/j.ijid.2018.01.034.
[47] A. Sobhan, J.-H. Oh, M.-K. Park, J. Lee, Reusability of a single-walled carbon nanotube-based biosensor for detecting peanut allergens and Y. enterocolitica, Microelectron. Eng. 225 (2020) 111281, https://doi.org/10.1016/j.mee.2020.111281.
[48] L. Martínez, L.G. Carrascosa, Y. Huttel, L.M. Lechuga, E. Román, Influence of the linker type on the Au-S binding properties of thiol and disulfide-modified DNA self-assembly on polycrystalline gold, Phys. Chem. Chem. Phys. 12 (2010) 3301–3308, https://doi.org/10.1039/b924504a.
[49] O. Georgacopoulos, N.S. Nunnally, N. Le, C. Lysen, R.M. Welsh, M. Kordalewska, D. S. Perlin, E.L. Berkow, D. Joseph Sexton, Performance evaluation of culture-independent sybr green candida auris quantitative PCR diagnostics on anterior nares surveillance swabs, J. Clin. Microbiol. 58 (2020), https://doi.org/10.1128/JCM.00690-20.
[50] M. Malczynski, N. Dowllow, S. Rezaeian, J. Rios, L. Dirnberger, J.A. Zembower, A. Zhu, C. Qi, Optimizing a real-time PCR assay for rapid detection of Candida auris in nasal and axillary/groin samples, J. Med. Microbiol. 69 (2020) 824–829, https://doi.org/10.1099/jmm.0.001207.
[51] Z. Shabaninejad, F. Yousefi, A. Movahedpour, Y. Ghasemi, S. Dokanehiifard, S. Rezaei, R. Aryan, A. Savardashtaki, H. Mirzaei, Electrochemical-based biosensors for microRNA detection: nanotechnology comes into view, Anal. Biochem. 581 (2019) 113349, https://doi.org/10.1016/j.ab.2019.113349.
[56] M. Yamamoto, M.M. Alshahni, T. Tamura, K. Satoh, S. Iguchi, K. Kikuchi, M. Mimaki, K. Makimurab, Rapid detection of candida auris based on loop-mediated isothermal amplification (LAMP), J. Clin. Microbiol. 56 (2018), https://doi.org/10.1128/JCM.00591-18.
[57] R.J. de Oliveira, Stochastic diffusion framework determines the free-energy landscape and rate from single-molecule trajectory, J. Chem. Phys. 149 (2018) 234107, https://doi.org/10.1063/1.5052142.
[58] L.M. Sousa, W.A. Souza, D.A. Paixão, R.B. Fazzi, D.Y. Tezuka, C.D. Lopes, Z. A. Carneiro, M.B. Moreira, M. Pivatto, A.V.G. Netto, S. de Albuquerque, F. B. Ferreira, R.J. De Oliveira, J.A.L.C. Resende, R.C. Lino, R.J. De Oliveira Júnior, A. M. Da Costa Ferreira, W. Guerra, DNA binding, cleavage, apoptosis and cytotoxicity studies of three heteroleptic nickel complexes bearing β-diketones, Inorg. Chim. Acta. 511 (2020), 119824, https://doi.org/10.1016/j.ica.2020.119824.
[59] J.M.R. Flauzino, R.C.S. Peres, L.M. Alves, J.G. Vieira, J.G. dos Santos, A.G. Brito-Madurro, J.M. Madurro, DNA electrochemical biosensor for detection of Alicyclobacillus acidoterrestris utilizing Hoechst 33258 as indicator, Bioelectrochemistry 140 (2021) 107801, https://doi.org/10.1016/j.bioelechem.2021.107801.
[60] F. Silva, S. Vieira, L. Goulart, J. Boodts, A. Brito-Madurro, J. Madurro, Electrochemical investigation of oligonucleotide-DNA hybridization on poly(4-methoxyphenethylamine), Int. J. Mol. Sci. 9 (2008) 1173–1187, https://doi.org/10.3390/ijms9071173.
[61] I. Piroeva, S. Atanassova-Vladimirova, L. Dimowa, H. Sbirkova, G. Radoslavov, P. Hristov, B.L. Shivachev, A simple and rapid scanning electron microscope preparative technique for observation of biological samples: application on bacteria and DNA samples, Bulg Chem. Commun. (2013).
[62] R. Bjugn, P.R. Flood, Scanning electron microscopy of human urine and purified tamm-horsfall's glycoprotein, Scand. J. Urol. Nephrol. 22 (1988) 313–315, https://doi.org/10.3109/00365598809180806.
[63] O. Corduneanu, A.-M. Chiorcea-Paquim, V. Diculescu, S.M. Fiuza, M.P.M. Marques, A.M. Oliveira-Brett, DNA interaction with palladium chelates of biogenic polyamines using atomic force microscopy and voltammetric characterization, Anal. Chem. 82 (2010) 1245–1252, https://doi.org/10.1021/ac902127d.
[64] J.M.R. Flauzino, E.L. Pimentel, L.M. Alves, J.M. Madurro, A.G. Brito-Madurro, A novel and reusable electrochemical genosensor for detection of beef adulteration, Electroanalysis 33 (2021) 296–303, https://doi.org/10.1002/elan.202060029.